

Spin-orbit and lattice coupling dynamics properties on enhanced Raman shift of perovskite films by resonance magnetic phase microscopy

REN R*, YJ REN, XUAN LI, ZHONGXIA ZHAO, DANAN R, RUIQI LU
Department of optics inf., Xi'an Jiao Tong University, Xian 710054, China

The distinct Raman active phonons in orthorhombic LSMO films heterojunctions were present by Raman spectroscopy of 325 nm and 512nm laser by the spin-orbit-lattice dependence of frequency performances in scattering configurations. The results show that high frequency mode structure and the perovskite symmetry phonon peaks is caused by anomalies tilt of MnO_6 octahedron. The spin-orbit transfer of $d_{x^2-y^2}$ orbit dynamics is based on crystal structure stabilized $d_{3z^2-r^2}$ orbit. The dynamics energy gain achieved by the ferro-orbital ordering, strong crystal field, spin-orbital competition and charge order of energy band splitting. The LSMO/ZnO junction display excellent junction behavior over the temperature range of 77–300 K and exhibit the strong crystal field and orbital canting.

(Received May 14, 2015; accepted October 28, 2015)

Keywords: Junction magnetoresistance, Spin-orbit, Carrier injection, MIT transition, Raman shift

1. Introduction

LaSrMnO_3 colossal magnetoresistance oxides are the most promising materials of the orbital degrees of freedom as well as orbital subsystem at different doping level and structure in studying the complex phase dynamics. [1] The doped manganese oxides $\text{La}_{0.7}\text{Sr}_{0.3}\text{MnO}_3$ (LSMO) displays competition coupling of spins, charge, orbit, and lattice order because of its pronounced two-dimensional structural and electronic characteristics. With reducing temperature the ferromagnetic samples exhibit cooperative Jahn-Teller distortion. [2,3] Further cooling a transition from a paramagnetic insulating (PI) to a ferromagnetic (FM) state was occurred at T_c where the resistivity begin to reduce. Also, ZnO is a most popular semiconductor material with a wide band gap (3.37 eV) and large exciton binding energy (60 meV). [4,5] The low dimensional nano-heter-junction of LSMO changes the orbital and spin dynamics [6].

LSMO crystallizes in the perovskite type tetragonal structure $R3C$, with O(1) in plane and O(2) apical oxygen sites as some high- T_c cuprates [7]. In LSMO, Raman scattering is sensitive for the active phonon modes and stretching modes of both local and spatially coherent structural changes. The MnO_2 magnetic layers are stacked along the c axis and separated by LaO_2 , SrO_2 plane [8]. LSMO is known to be an interesting structure to research the ferro-orbital ordering of $d_{3z^2-r^2}$ orbitals and a C-type antiferromagnetic (AF) spin ordering below T_N [9], which charge and orbital ordered phase caused by

electron-phonons dynamics. [10]

Ferroelectric ZnO contains transition metal ions with unpaired d electrons. The heterojunction $\text{ZnO}/\text{La}_{0.7}\text{Sr}_{0.3}\text{MnO}_{3+\sigma}$ nanostructure is good candidate for fabrication of nanometer-sized optoelectronic devices. It is expected that structural changes and spin-orbital magnetic order will influence the electron-phonon spectra. The doped strontium $\text{La}_{0.7}\text{Sr}_{0.3}\text{MnO}_{3+\sigma}$ and ZnO junctions with carrier transfer exhibit photoinduced resistance and colossal magnetoresistance (CMR) effect. [1]

So far, Zheng, RK focused on effects of the strain induced by ferroelectric poling of LaMnO_3 grown on $\text{Pb}(\text{Mg}_{1/3}\text{Nb}_{2/3})\text{O}_3$ - PbTiO_3 substrates, and explored the strong coupling of charge carriers to JT distortion for understanding the effects of the substrate-induced strain in manganite thin films. [12] The transport behavior accompanying domain switching was reported in $\text{La}_{0.1}\text{Bi}_{0.9}\text{FeO}_3/\text{La}_{0.7}\text{Sr}_{0.3}\text{MnO}_3$. [15] Arindam used nonequilibrium magnetotransport spectroscopy to explore spin polarization at low temperature and a strong sensitivity of such polarization to magnetic fields. [13] Those groups have reported the growth of two dimensional heterojunction nanostructures using different methods. The lower dimensionality changes the orbital and spin coupled dynamics, and either related to more pronounced fluctuations or raise orbital degeneracies. [2] Although other Raman spectra have been reported, there are few perovskites spectra information on the lattice dynamics in heterojunction films as well as to analyze more specific aspects of phonon-electrons interactions. The LSMO has a

tetragonal structure structure, ($I4/mmm$) space group, with O(1) in-plane and O(2) apical oxygen sites. The presence ZnO [14] of the d electrons can result in a relatively small gap and give rise to a concentration of charged impurities and defects.

In this letters, we reported Raman scattering studies of ZnO/LSMO/LaAlO heterojunction with different nano-structure to investigate spin-lattice structure dynamics of IM phase transition. We prepared multi-crystal LSMO/ZnO to introduce MR and carrier injection. A temperature dependence of positive magnetoresistance was observed in this junction that has some special properties of ferromagnetic semiconductor, [8,9] multilevel resistive switching, [10] positive colossal magnetoresistance, [11, 12] colossal electroresistance, [13] manganite tunnel junctions[14], high magnetic sensitivity and ultraviolet fast-response.[15]

2. Model and experiment

The fabricated heterostructure LaSrMnO and ZnO thin films were grown on LaAlO substrate by pulse laser deposition method. The LSMO thin film was fabricated on LaAlO₃ (100) at 800°C and oxygen pressure. The ZnO film about 75nm was deposit masked on LaSrMnO (100). The structure of the target and the orientation of the deposited film were studied by XRD (Bruker D8 Advance XRD).

The distortions of the MnO₆ octahedra were lowered by Mn⁴⁺/Mn³⁺ ratio. The ZnO/ LSMO structure was characterized by x-ray diffraction pattern shown in Fig. 1(a)(b)(c). Raman spectra of films were measured in a quasiback scattering with $\lambda = 514\text{nm}$ of Ar laser, 325nm laser with the 8mW and were collected by Raman spectrometer (HR800,HORZBA,Jobin Yvon) and a nitrogen cooled charge-coupled device detector. The grain refinements showed LSMO sample crystal belong to the hexagonal perovskite structures (space group:R-3C). When σ increases, a distorted orthorhombic O phase changes to a pseudocubic one (σ) then transits to a rhombohedral one.

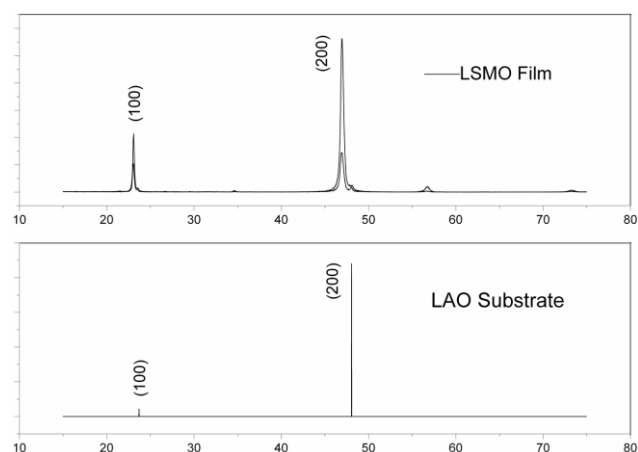
3. Results and discussion

The XRD image indicated that the ZnO (100) (002) (101) (102) (110) (103) (200) diffraction peak occurred at $2\theta = 66.15^\circ$, $2\theta = 56.4^\circ$, $2\theta = 47.3^\circ$, $2\theta = 34.37^\circ$, $2\theta = 36.09^\circ$, $2\theta = 62.78^\circ$ and $2\theta = 31.59^\circ$, while the La_{0.7}Sr_{0.3}MnO_{3+ σ} (100) and (200) diffraction peaks occurred at $2\theta = 23^\circ$ and $2\theta = 47^\circ$. The ZnO film is $2\theta = 34^\circ$ for the (002) orientation with the structure of a hexagonal wurtzite. This LSMO film (100) with the LAO substrate had the multi-crystal structure. The diffraction peak of La_{0.7}Sr_{0.3}MnO₃/ZnO was matched with the LAO

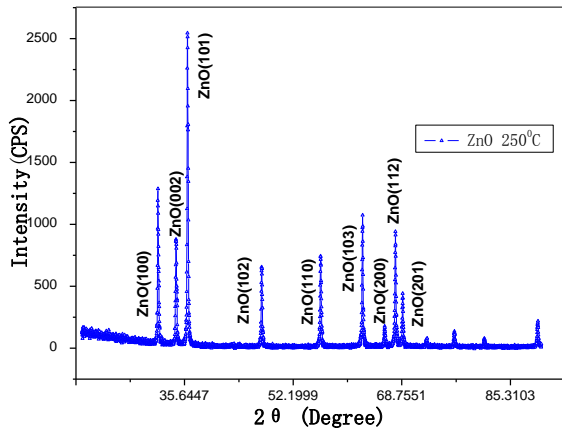
substrate. The results indicated that the La_{0.7}Sr_{0.3}MnO₃ and ZnO thin films had better epitaxial characters respectively.

Raman spectra displays the O and La(Sr) vibrations with shifting along the a and b axis with E_g symmetry shown in Figure. For LSMO the space group R3C, the group analysis yields four Raman-active phonon modes: The Mn³⁺-O-Mn⁴⁺ and La(Sr)O₂ extending modes have stretched along the c axis.

Measured ZnO and LaSrMnO Raman shift, the factor group analysis displays four Raman active phonon modes: 620,490,220 and 150cm⁻¹. A large softening of Mn-O bond stretching modes below the Curie temperature and a broadened, loose multiphonon feature indicates a fluctuating orbital state in FMI sample. When the LSMO has tiny crystal lattice distortion, the size of Mn³⁺ and Mn⁴⁺ atom corresponds to expansion Mn-O chain. LaSrMnO E (TO₁) soft mode is in the first brillouin zone. The stretching leads to rotating, tilt of octahedral and vibration of heavy rare metals. These forbidden peaks are weak in intensity but show a well defined symmetry. We can find the phonon modes dependence in frequencies, which rules out impurities and defects as a possible origin. The group analysis yields four Raman active phonon modes: Mn-O(2) and (La,Sr)-O(2) stretching modes and O(2) and (La,Sr) vibrations with displacements along the a and b axes with E_g symmetry. We can measure LaSrMnO Raman spectrum contains ten kinds of typical single mode A₁ (LO₃),B₁+E, A₁ (TO₂), A₁ (TO₁) E (TO₂), A₁ (two-to-three) E (LO₂), E (two-to-three), E (LO₁) and E (TO₁).



(a) X-ray diffraction of La_{0.7}Sr_{0.3}MnO₃/LAO



(b) X-ray diffraction of ZnO film at 250°C

Fig. 1(a)(b) X-ray diffraction pattern of ZnO/La_{0.7}Sr_{0.3}MnO₃/LAO heterostructure. The insets shows the (100) and (200) peaks of the LSMO film and LAO substrate. X-ray diffraction of ZnO heterostructure at 250°C

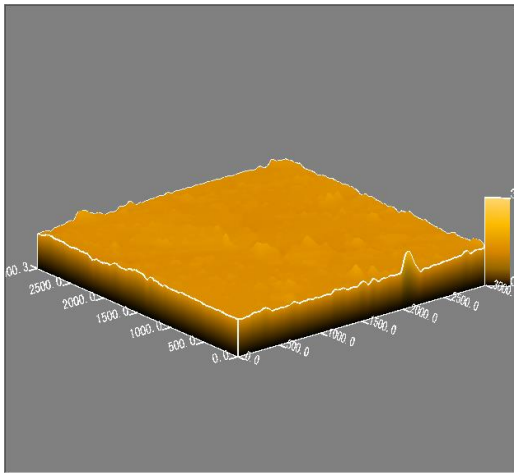


Fig. 2 Magnetic phase microscopy of LSMO film. The thickness dependence on Raman scattering in polarization in LSMO.

Fig.2 also displays Magnetic phase microscopy of LSMO film which the respective spectrum in four polarization, where a and b correspond to the polarization of incident or scattering light along the MnO direction. We observed the LSMO plane polarization. These scattering peaks are formed by $A_{2g}+B_{2g}$, $B_{1g}+A_{2g}$, $A_{1g}+B_{2g}$ and $A_{1g}+B_{1g}$, symmetries, respectively. The magnetoresistance ferr-electricity phase transition of multilayers heterjunction could be revealed by lattice vibrated mode of spectra as well as the dielectric polarization and resistance-temperature properties could be explored.

Fig. 3 shows the Raman scattering spectra He-Cd laser of LSMO films with wavelength of 325 nm. The frequencies of 602, 570, and 580 cm^{-1} corresponds to orthogonal cubic phase, which is MnO_6 octahedral

stretching with the symmetric and antisymmetric vibration characteristic peaks. The scattering peaks at 570 cm^{-1} 580 cm^{-1} is Jahn Teller transition phase. The characteristic peaks near at 310 cm^{-1} is for the tilt vibration of MnO_6 octahedral. It corresponds to the bond angle changes of $\text{Mn}^{3+}\text{-O-Mn}^{4+}$. We observe weak A_{1g} phonon signals at the frequencies of 203 cm^{-1} and 310 cm^{-1} as in (cc) polarization. The octahedral tilt MnO_6 vibration peak is at 310 cm^{-1} which is a A_{1g} symmetry. The scattering peaks of LSMO 95 nm film appear at 480 cm^{-1} , 320 cm^{-1} , 675 cm^{-1} , 542 cm^{-1} and 602 cm^{-1} .

We observed lattice structure and physical properties ZnO/ LSMO as a result of changes of crystal field, temperature, strain, and interface roughness. The LSMO film thickness increases, while the axis peak of rhombohedral phase gradually enhances. The LSMO characteristic peak at frequency 702 cm^{-1} exhibits rhombus antisymmetric stretching mode. The activated peaks are pronounced in the middle frequency range of 190-490 cm^{-1} . Because the Mn-O(1) distance is shorter than Mn-O(2), the Mn-O(1) frequencies are higher than 400 cm^{-1} of Mn-O(2) mode. From 95 nm to bulk, A_{1g} characteristic peak move to the high frequency direction that those wave number has shift. With increasing characteristic vibrational energy A_{1g} , the A_{1g} peak shifts. The anti-symmetric stretching mode is from 675 cm^{-1} to 649 cm^{-1} . The vibration energy of MnO_6 octahedral stretching decreases because of the a axis increase. The former modes are similar to excitations of LSMO with splitting of the charge-exchange type and orbital order. The LSMO out plane $d_{3z^2-r^2}$ orbital character is enhanced at low temperature which is due to an increase of the tetragonal distortion of octahedron. The middle frequencies correspond to MnO_6 tilting. The high frequencies correspond to MnO stretching. Moreover, Raman scattering peak, as the film thickness reduces from bulk to 95 nm thickness. The peak near 310 cm^{-1} moves to low wave number. We measure harmonic oscillator model of lattice. The c axis gradually decreases due to a axis rise up and c axis down. The adjacent angles between MnO_6 were improved. The low frequencies correspond to MnO spinic and rare element phonon vibration.

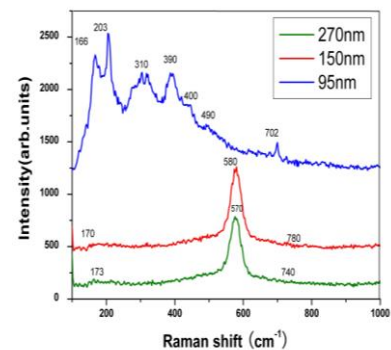


Fig. 3. Raman scattering spectrum of LSMO film with 325 nm excited laser. The thickness is dependence of Raman scattering in polarization LSMO

The film performs the coexistence of double phase structures. There are rhombohedral phase and Jahn Teller distorted peak at 640 and 703 cm⁻¹. The first-order ZnO Raman spectra involve lattice vibration modes near Bloch zone, and optical phonons including 1A₁, 2B₁, 1E₁, and 2E₂. The distortion of octahedra LSMO leads to spin-orbit coupling to crystal lattice, as the result of lattice and spin coupling between t_{2g} and e_g orbitals.[15] This implies that the hole possesses out-of-plane d_{3z²-r²} orbital, while the corresponding number of electrons occupies in-plane d_{x²-y²} orbitals.

The experiment displays that 217 cm⁻¹, and 449 cm⁻¹ are related to LSMO A_{1g} phonon signals. 560 cm⁻¹ is determined directly from the peak of A_{1g} symmetry, and low-frequency corresponds to O (2) oxygen. For 514 nm excited Ar⁺ laser, Jahn Teller at 703 cm⁻¹ emerges in the series of distorted peaks at 630, 640 and 703 cm⁻¹. The characteristic peak at 703 cm⁻¹ with 325 nm excited laser is rhombohedral phase with no Jahn Teller distorted peak. The 300 and 356 cm⁻¹ peaks are origin from many phonon scattering. The ground state of AF and upper state (S = 2, S₂ = 2) to (S = 2, S₂ = 1) emission are obtained by half elastic scattering appeared near the T_N according to the double spin-flip transition. The exchange degrees of adjacent Mn spin are available shown as J = (2nI - 1). I is the spin quantum number, n is the number of nearest neighbor spin, J shows the situation of Mn spin exchange. Raman peak width, intensity, and shape asymmetry reflect the heterojunction structure information, interface and electronic characteristics of ZnO thin film at low temperature. The peak (E₂) at 430-432 cm⁻¹ shows that film thickness and strain stress changes lattice. Moreover, the temperature dependence of the ZnO/LSMO device resistance properties under different magnetic fields was measured. The resistance reached the maximum values of about 25.948% at 0.5 T, 190 K, 24.89% at 0.3 T, 175 K, and 22.764% at H = 0.1 T and T = 145 K. The spin polarization transport of double exchange mechanics are observed in LSMO metal insulator transition, which the substitution of divalent alkaline earth element leads to the mixed valence state of Mn: Mn³⁺t_{2g} 3d and Mn⁴⁺t_{2g} 3d. A temperature driven orbital occupation of diluted d_{x²-y²} is in the background of crystal field d_{3z²-r²}. It is called spin coupling strongly to the lattice. Moreover, the Mn³⁺-O²⁻-Mn⁴⁺ coupling produces ferromagnetic strong correlation through the charge hopping leading to the anomalous magnetization. The vibronic-induced cooperative JT effect blurs the e_g bands and allows the Mn³⁺ e_g electrons to hop into the empty orbital states [10-27].

4. Conclusions

In summary, we have reported distinct Raman active phonons scattering spectrum on single orthorhombic LSMO films Raman and multilayer heterojunctions LSMO of spin-orbit-lattice coupling. The spin-structure dynamics indicated that orbital coupling is origin of lattice anomalous.

We observe high frequency mode structure and the perovskite symmetry phonon peaks is caused by anomalies tilt of MnO₆ octahedron. The carrier transport spin-orbit dynamic is made by the lattice distortion in ZnO/La_{0.7}Sr_{0.3}MnO_{3-σ}. The junction resistance properties are adjusted by spin-orbit, magnetic and lattice field. The spin-orbit transfer of d_{x²-y²} orbitals dynamics is based on crystal structure stabilized d_{3z²-r²} orbit. The junction resistance due to field effect and alteration energy band, which are deformed by magnetic structure, crystal structure, and carrier concentration. Our measure is attributed to the further understanding of ferro-orbital ordering, strong crystal field, spin-orbital competition and charge order of energy band splitting and development of photoinduced demagnetization and positive CMR device.

*Supported by the National Natural Science Foundation of China under Grant 61574115, 10775111

References

- [1] A Machida, T. Watanuki, D. Kawana, *Physical Rev. B*, **83**(5), 054103, (2011).
- [2] C. Sen, G. Alvarez, E. Dagotto, *Phys. Rev. Lett.* **98**, 127202 (2007).
- [3] C. Zener, *Phys. Rev.* **82**, 403 (1951).
- [4] M. F. Cetin, P. Lemmens, V. Gnezdilov, *Phys. Rev. B*, **85**(19), 195148 (2012).
- [5] K. De, S. Das, A. Roy, *J. Appl. Phys.* **112**(10), 103907 (2012).
- [6] V. Gnezdilov, J. Deisenhofer, P. Lemmens, *Low Temp. Phys.* **38**(5), 419 (2012).
- [7] A. Antonakos, E. Liarokapis, G. H. Aydogdu, *J. of Magnetism and Magnetic Materials*, **323**(5), 620 (2011).
- [8] R. K. Zheng, Y. Wang, H. L. W. Chan, *J. Appl. Phys.* **108**(12), 124103 (2010).
- [9] R. K. Zheng, Habermeier, *Phys. Rev. B*, **81**(10), 104427 (2010).
- [10] A. Sawa, T. Fujii, M. Kawasaki, Y. Tokura, *Appl. Phys. Lett.* **85**, 4073 (2004).
- [11] X. P. Zhang, B. T. Xie, Y. S. Xiao, B. Yang et al, *Appl. Phys. Lett.*, **87**, 072506 (2005).
- [12] R. K. Zheng, H. U. Habermeier, H. L. W. Chan, *Physical Review B*, **81**(10), 104427 (2010).
- [13] N. Zhang, T. Geng, H. X. Cao, J. C. Bao, *Chin. Phys. B*, **17**, 317 (2008).
- [14] T. A. Sidorov, *Russian J. of Inorganic Chemistry*, **58**, 6 (2013).
- [15] J. R. Sun, *Appl. Phys. Lett.* **101**(15), 152901 (2012).
- [16] S. Mori, R. Shoji, N. Yamamoto, T. Asaka, Y. Matsui, Y. Moritomo, *Physical Rev. B*, **67**(1), 012403 (2003).
- [17] C. Barraud, P. Seneor, R. Mattana, S. Fusil, Karim Bouzehouane, C. Deranlot, P. Graziosi, L. Hueso, *Nature Physics*, **6**, 615 (2010).

- [18] R. Lengsdorf, M. Ait-Tahar, S. S. Saxena, M. Ellerby, D. I. Khomskii, H. Micklitz, T. Lorenz, *Phys. Rev. B*, **69**(14), 140403 (2004).
- [19] P. Kumar, R. Mahendiran, *Applied Phys. letters*, **106**(14), 142401 (2015).
- [20] R. Vonhelmolt, J. Wecker, K. Samwer, L. Haupt, K. Barner, *J. Appl. Phys.* **76**, 6925 (1994).
- [21] P. Lemmens, G. Guntherodt, C. Gros, *Phys. Rep.* **375**, 1 (2003).
- [22] R. Ren, L. Xuan, W. Weiren, *Optoelectron. Adv. Mater.-Rapid Comm.*, **7**(7-8), 593 (2013).
- [23] R. Ren, L. Xuan, W. Weiren, *J. Appl. Phys.* **114**(13), 133705 (2013).
- [24] X. Jin, H. S. Sheng, *J. Clinical Neurophysiology*, **29**(3), 230 (2012).
- [25] R. Ren, Y. J. Ren, W. R. Wang, X. Li, *Science of advanced materials*, **6**(6), 1255 (2014).
- [26] X. Jin, S. Z. Zhao, H. S. Zhang, *Clinical EEG and Neuroscience*, **42**(1), 53 (2011).
- [27] R. Ren, W. R. Wang, Xuan Li, *Physica Scripta*, **89**(3), 035601 (2014).

*Corresponding author: ren@mail.xjtu.edu.cn